Iranian Journal of Materials Forming 13 (2) (2026) 13-22

Online ISSN: 2383-0042

IJMF

Iranian Journal of Materials Forming

Journal Homepage: http://ijmf.shirazu.ac.ir

Research Article

Effects of Laser Output Power and Scanning Speed on Geometrical Deformation During the Laser Tube Bending Process of Perforated Tubes

Mehdi Safari * and Danesh Daneshpour

Department of Mechanical Engineering, Arak University of Technology, Arak 38181-41167, Iran

ARTICLE INFO

Article history:

Received: 7 October 2025
Reviewed: 13 December 2025
Revised: 19 December 2025
Accepted: 21 December 2025

Keywords:

Laser bending process
Perforated tube
Ovality
Thickness variations

Please cite this article as:

Safari, M., & Daneshpour, D. (2026). Effects of laser output power and scanning speed on geometrical deformation during the laser tube bending process of perforated tubes. *Iranian Journal of Materials Forming*, *13*(2), 13-22. https://doi.org/10.22099/IJMF.2025.54470.1355

ABSTRACT

In this work, the laser bending process of perforated tubes is investigated using numerical simulations. For this purpose, the finite element software ABAQUS is used. The effects of key process parameters such as laser output power (LOP) and laser scanning speed (LSS) on the main displacement of the free edge (desired response) and the lateral displacement of the free edge, cross-section ovality, ovality of holes located along the laser irradiating path, and thickness variations in the tube wall (undesired responses) are investigated. The results show that the main displacement of the free edge of the laser-bent tube increases with an increase in the LOP and a decrease in the LSS. Similarly, the lateral displacement of the free edge of the laser-bent tube increases with an increase in the LOP and a decrease in the LSS. Other undesired effects, including cross-section ovality, ovality of the holes located at the laser irradiating path, and thickness variations in the tube wall, also increase with an increase in the LOP and a decrease in the LSS.

© Shiraz University, Shiraz, Iran, 2026

1. Introduction

Perforated tubes are hollow cylinders characterized by a series of uniformly or variably spaced holes, known as perforations, which are intentionally created within the tube structure. The configuration of these perforations not only serves functional purposes but also influences physical properties such as weight, flow dynamics, and mechanical strength. The unique properties of perforated tubes enable their use in a wide array of applications across various sectors such as filtration systems, architectural elements, chemical and process engineering, aerospace and automotive, agricultural applications, among others. The laser tube bending process (LTBP) is an innovative manufacturing technique that utilizes laser irradiation to induce localized heating, resulting in the bending of tubes

* Corresponding author
E-mail address: m.safari@arakut.ac.ir (M. Safari)
https://doi.org/10.22099/IJMF.2025.54470.1355

Published by Shiraz University. This is an open access article under the CC BY-NC-ND license (http://creativecommons.org/licenses/by-nc-nd/4.0/).

without the need for traditional tooling. This method offers advantages such as reduced spring-back and improved accuracy, making it suitable for various applications in industries like aerospace and automotive. Key aspects of LTBP include the influence of process parameters, the effects of different irradiation schemes, and advancements in material treatment aimed at enhancing forming performance. In recent years, researchers have conducted studies on laser-assisted tube bending, some of which are highlighted below.

Safari et al. [1] discussed the effect of process parameters and their interactions on the bending angles of laser-bent tubes. Their results showed that the main bending angle and the lateral bending angle increased with increasing laser output power (LOP), and reducing scanning speed. An experimental investigation was carried out by Imhan et al. [2] to improve the LTBP by enhancing the absorption coefficient of the material. A formula for the bending angle in LTBP was proposed by Hao [3] based on plastic mechanics and verified by experimental tests. It was seen that the bending angle depends on LOP, LSS, dimensions, and material properties. In another work, an analytical investigation was conducted by Imhan et al. [4] to analyze the effects of average LOP and LSS on the LTBP. Their analytical results were verified experimentally. A thorough experimental investigation was carried out on the laser tube bending procedure by Imhan et al. [5], in which the evolution of material properties during processing was also considered. In their work, Hao and Li's analytical framework was modified by incorporating a correction coefficient. Laser bending of tubes was realized numerically by Guan et al. [6]. They found that the relationship between the number of scans and the bending angle was approximately linear, while the bending angle varied with the laser spot diameter. Imhan et al. [7] compared the LTBP with laser sheet forming to develop a better understanding of the laser forming process. Hao and Gai [8] proposed a pattern for LTBP by varying the bending direction continuously, which is suitable for low ductility material and thin-walled tubes. Li and Yao [9] proposed a formula for the bending angle to better understand the deformation characteristics in LTBP. Khandandel et al. [10] proposed a cooling strategy during LTBP to eliminate the disadvantages of axial and circumferential scanning, and the bending angle behaviors were experimentally investigated. Li et al. [11] studied the effect of processing parameters such as LOP and LSS on the bending angle in the LTBP experimentally. A three-dimensional finite element model for the LTBP was developed by Guan et al. [12] using MSC/Marc software. Zhang and Liu [13] performed a numerical investigation on tubes with rectangular cross-section, including model discretization.

As evidenced by the literature review, all existing research on LTBP has focused on non-perforated tubes. According to the authors' knowledge, no research has been conducted on the LTBP of perforated tubes. The laser bending of perforated tubes is fundamentally distinct from that of solid tubes due to the synergistic interaction of three key effects introduced by the perforations. These Perforations create mechanical discontinuities, breaking the continuous load path and making the structural response highly dependent on the ligament geometry between holes. This effect is compounded by heat concentration, where reduced thermal mass around perforations leads to rapid, non-uniform temperature fields that deviate sharply from the smooth gradients observed in solid tubes. Crucially, these geometric discontinuities also induce stress concentration, focusing both thermal and mechanical stresses at the perforation edges, which dramatically alters yield localization and plastic strain distribution. Therefore, this paper numerically investigates the LTBP of perforated tubes using the finite element software ABAQUS. Given the absence of prior research in this area, the results of this study provide foundational insight and initiate a new research direction for understanding and optimizing the laser tube bending of perforated structures.

2. Numerical Simulations

During the laser tube bending procedure, there is an interaction between the temperature and displacement fields. Consequently, numerical analyses have employed

the finite element method to conduct thermal and mechanical evaluations of the laser forming process. For this analysis, the ABAQUS implicit code has been utilized. In these simulations, the mechanical and thermal calculations can be treated separately. This separation is justified due to the minimal energy loss from plastic deformation when compared to the significant laser energy involved in the process. In the decoupled approach, thermal analysis is conducted initially to determine the temperature distribution, which is then applied as thermal loading in the subsequent mechanical analysis. Essentially, a comprehensive thermal computation is completed up to the final time, after which the temperature history is incorporated into a purely mechanical computation. The ABAQUS simulations allow for the determination of fields related to thermal stress, temperature, and displacement. Fig. 1 illustrates a schematic representation of the laser bending process of a perforated tube.

The initial tube is made of mild steel with dimensions of 140 mm in length, 18 mm in outer diameter, and a thickness of 1 mm. During the laser bending operation, both the temperature and deformation in the locally heated area exhibit rapid fluctuations over a brief period, leading to significant temperature and stress gradients. To achieve greater accuracy, brick elements are utilized, allowing for precise calculations at integration nodes. A fine mesh is imperative around the laser beam trajectory to accurately capture these steep gradients. At least four integration points in the thickness direction are required for reliable results. To minimize the overall number of elements in the simulation, a coarser mesh is applied in areas outside the heating zone. To reduce the influence of element size on numerical accuracy, a mesh independence study was performed to determine the optimal element size.

Fig. 2 depicts a tube with an appropriate mesh configuration for the laser bending simulation.

As illustrated, denser meshes are positioned near the heat source for enhanced accuracy, while coarser meshes are utilized farther away to decrease computational time. Since the simulation in this work is uncoupled, the thermal analysis is first performed, and the resulting temperature history is subsequently applied as a thermal load in the mechanical solution. In the mechanical solution, one side of the tube is completely clamped and the other side is completely free. For the mechanical analysis, the twenty-node 3D element C3D20 is employed, which avoids shear locking and hourglass issues, making it well-suited for bending processes like laser bending. In the thermal analysis, the twenty-node element DC3D20 is utilized. In the simulation of the LTBP, the laser beam is modeled as a surface heat flux. Consequently, the ABAQUS user subroutine DFLUX is employed to define this surface heat flux, accurately representing the heat source in the laser forming process. The DFLUX subroutine is implemented to numerically characterize the heat flux density, geometry, dimensions, and scanning velocity. The heating load is automatically applied to the relevant element faces. The distribution of

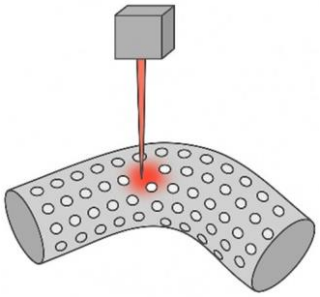

Fig. 1. Schematic representation of the laser bending process of a perforated tube.

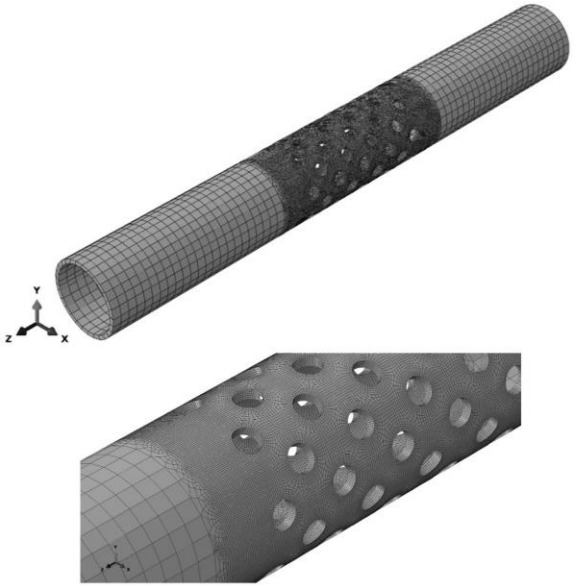

Fig. 2. A tube with an appropriate mesh configuration for the laser bending simulation.

surface heat flux is calculated using the following formula [14]:

$$Q(x,z)=\frac{3\eta P}{\pi R^2}Exp\left(-3\left(\left(\frac{x}{R}\right)^2+\left(\frac{z}{R}\right)^2\right)\right) \quad (1)$$

The parameter η represents the absorption coefficient of the laser-irradiated surface (0.6 in the simulations), while P denotes the laser power. The symbol R corresponds to the laser beam radius on the sheet metal surface, and x and z indicate the positional distances from the laser beam's central axis. Heat exchange at the boundaries is governed by natural convection and thermal radiation mechanisms. According to Newton's law of cooling, the convective heat transfer follows a linear relationship, where the rate of heat loss per unit surface area (Wm^{-2}) caused by convection is given by Eq. 2 [14]:

$$q_c = h_c(T_s - T_a) \quad (2)$$

Here, h_c represents the convective heat transfer coefficient (10 W/m^2K in the simulations), T_s denotes the temperature of the laser-irradiated surface, and T_a stands for the ambient temperature. The rate of heat loss per unit area (Wm^{-2}) resulting from thermal radiation can be formulated as Eq. 3 [14]:

$$q_r = 5.67\times10^{-8}\varepsilon(T_s^4 - T_a^4) \quad (3)$$

Where the surface emissivity (0.5 in the simulations), which varies based on surface conditions and the temperature of the metal plate, is specified. For the mechanical analysis, necessary constraints are applied to prevent rigid-body movement. The material properties of mild steel, including thermal conductivity, specific heat, Young's modulus, expansion coefficient, and yield stresses, are temperature-dependent, with the relevant data provided in Tables 1 and 2.

The same mesh configuration is utilized for both thermal and mechanical analyses. The simulations are conducted in two phases: first, the tube is exposed to the laser beam, and subsequently, it is cooled to ambient temperature, using the same convection coefficient for both heating and cooling phases. It is assumed that no water or gas jets are employed during the cooling phase. Fig. 3 presents representative thermal contour plots obtained from the numerical simulations of the LTBP for perforated tubes, while Fig. 4 illustrates the corresponding mechanical contour plots.

Table 1. Thermal properties of mild steel [14]

Temperature (°C)	Thermal conductivity (W/mm/°C)	Specific heat (kJ/kg/°C)
00	51.9E-3	486
100	51.1E-3	486
200	48.6E-3	498
300	44.4E-3	515
400	42.7E-3	536
500	39.4E-3	557
600	35.6E-3	586
700	31.8E-3	619
800	26.0E-3	691
900	26.4E-3	695
1000	27.2E-3	691
3000	120.0e-3	700

Table 2. Mechanical properties of mild steel [14]

Temperature (°C)	Elasticity modulus (N/mm^2)	Poisson's ratio	Expansion	Yield stress for e_p = 0 (N/mm^2)	Yield stress for e_p = 0.1 (N/mm^2)
20	0.206E+06	0.296	0.117E-04	344.64	422.64
100	0.203E+06	0.311	0.117E-04	331.93	409.93
200	0.201E+06	0.330	0.122E-04	308.30	386.30
300	0.200E+06	0.349	0.128E-04	276.07	342.57
400	0.165E+06	0.367	0.133E-04	235.22	290.22
500	0.120E+06	0.386	0.138E-04	185.77	230.77
600	0.600E+05	0.405	0.144E-04	127.71	162.71
700	0.400E+05	0.423	0.148E-04	68.55	96.05
800	0.300E+05	0.442	0.148E-04	64.35	84.35
900	0.200E+05	0.461	0.148E-04	46.65	60.65
1000	0.100E+05	0.480	0.148E-04	11.32	21.32
3000	0.100E+05	0.480	0.148E-04		

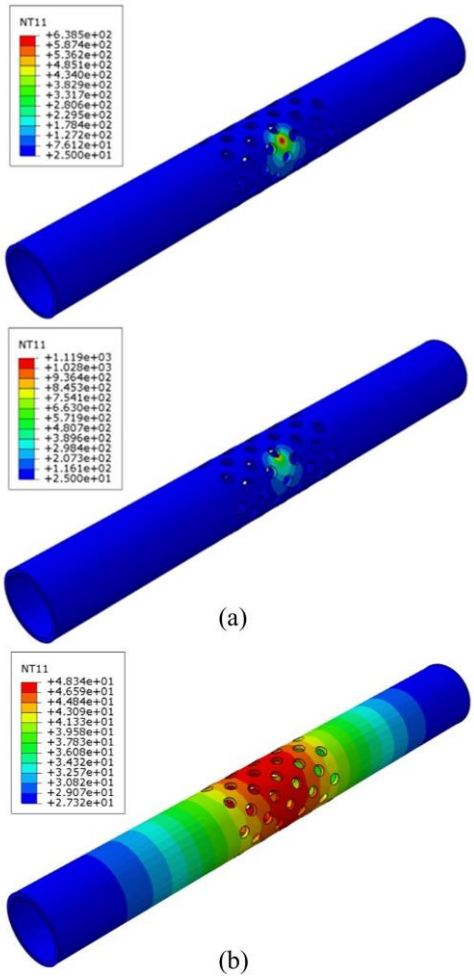

Fig. 3. Thermal contour plots of numerical simulations of LTBP of perforated tubes; (a) irradiating step, (b) cooling step.

In the LTBP, unwanted defects arise along with the primary bending mechanism, which can reduce the dimensional accuracy of the laser-bent tube. These unwanted defects are discussed in detail in the following sections.

2.1. Lateral bending

During laser tube bending process, an additional lateral bending angle is inadvertently generated alongside the primary bending angle, which is an unwanted effect. This occurrence adversely impacts the dimensional precision of the laser-bent tube. Further details are provided in reference [13].

2.2. Ovality

The phenomenon of ovality is primarily linked to the development of tensile stresses on the outer surface and compressive stresses on the inner surface within the heat-affected zone during the bending process. Further details are provided in reference [13]. The ovality percentage quantifies the distortion of the cross-sectional shape of a circular tube within the bending region. In practical applications, such distortions can result in turbulent flow for any fluid traveling through the tube. The roundness of the tube's cross-section can be described by the following equation:

$$Ovalization = \frac{D_{max} - D_{min}}{D} \times 100(\%) \quad (4)$$

In this expression, D_{max} and D_{min} denote the maximum and minimum average diameters of the deformed tube, respectively, while D refers to the original (undeformed) diameter of the tube.

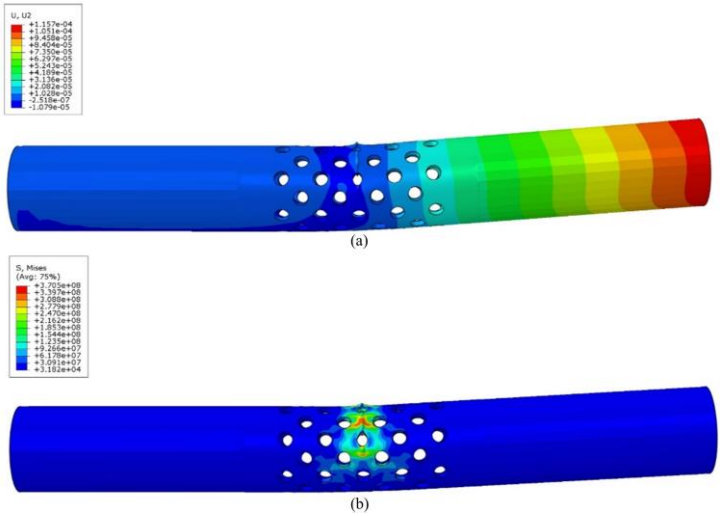

Fig. 4. Mechanical contour plots of LTBP of perforated tubes; (a) displacement of free edge, (b) equivalent Mises stress.

2.3. Thickness variations in the cross-section of laser-bent tube

The development of tensile stresses on the outer surface and compressive stresses on the inner surface during the bending process leads to changes in thickness after the laser bending operation. Further details are provided in reference [13]. For investigating the thickness variations in the LTBP, the thickness variation ratio (TVR) is defined as:

$$TVR = \frac{Thickness\ at\ highest\ point\ of\ intrados}{Thickness\ at\ lowest\ point\ of\ extrados} \quad (5)$$

2.4. Ovality of the holes located on the irradiating path

In the laser bending process of perforated tubes, the holes located along the laser beam path undergo slight dimensional changes and become elliptical during and after irradiation due to expansion and contraction. This phenomenon reduces the dimensional accuracy of the laser-bent tube. Fig. 5 shows examples of laser-irradiated holes in a perforated tube that have become elliptical as a result of irradiation.

3. Results and Discussion

At the beginning of this section, it is important to note that the simulations performed in this work, in terms of material properties, include mechanical and thermal properties of the tube, type of thermal-mechanical problem solving, boundary conditions, and loading are similar to those used for the laser-bent tube in reference [14]. The difference is that the tube geometry in reference [14] did not include perforations, whereas the present work considers a perforated tube. Therefore, considering that the simulations performed in reference [14] were confirmed by experimental results, it can be stated that the simulations performed in the present paper are also validated. However, the effects of the main process parameters such as LOP and LSS on the lateral displacement of the free edge, lateral displacement of free edge, cross-section ovality, hole ovality, and TVR are shown and discussed.

3.1. The effect of LOP

In Fig. 6, the effect of LOP on the main displacement of the free edge in the laser-bent perforated tube is shown. As observed, the main displacement of the free edge increases with an increase in the LOP.

Increasing LOP applies more heat energy to the tube per unit time. This raises the temperature in the irradiated region, causing a larger volume of material to reach the thermal plastic deformation zone. As a result, more material undergoes permanent deformation, leading to a larger bending angle. At low power levels, only a thin layer near the surface is plastically deformed. With higher power, this zone expands through the wall thickness, increasing the total curvature and bending angle. In Fig. 7, the effect of LOP on the lateral displacement of the free edge in the laser-bent perforated tube is shown. As observed, the lateral displacement of the free edge increases with an increase in the LOP.

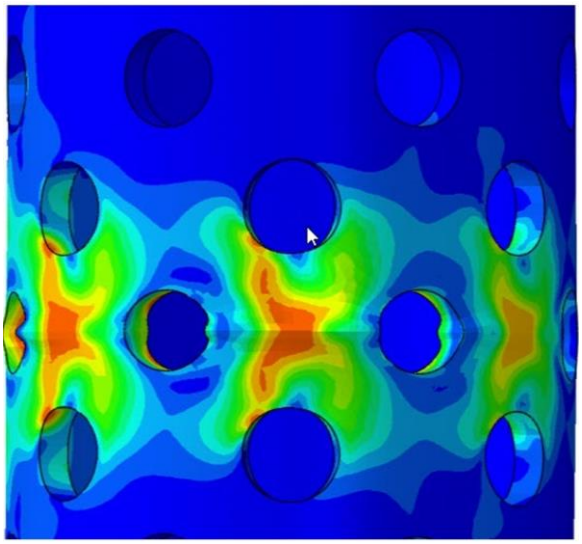

Fig. 5. Laser irradiated holes of a perforated tube that have become elliptical due to irradiation.

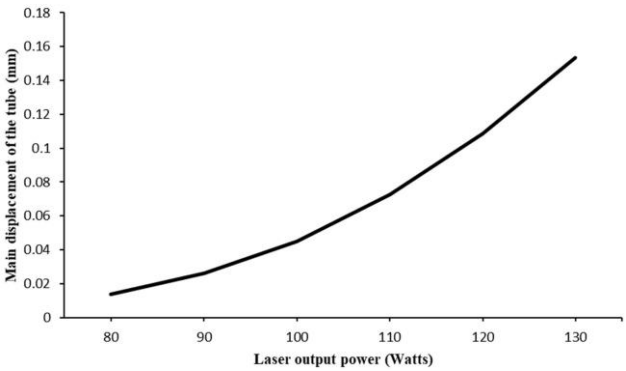

Fig. 6. The effect of LOP on the main displacement of the free edge in the laser-bent perforated tube.

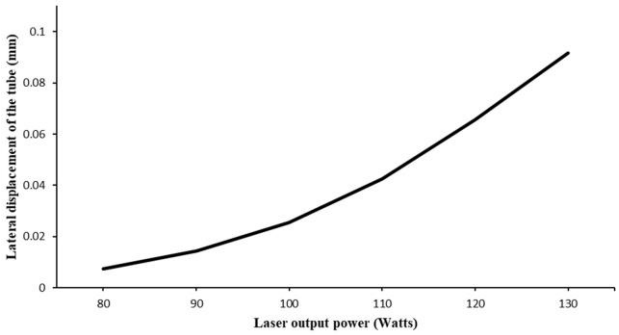

Fig. 7. The effect of LOP on the lateral displacement of the free edge in the laser-bent perforated tube.

The reason is that increasing LOP applies more energy to the surface. This produces a greater and more asymmetric temperature field, causing uneven thermal expansion between the irradiated and non-irradiated sides. The resulting unbalanced thermal stresses and bending moments lead to a larger lateral deviation of the tube. In Fig. 8, the effect of LOP on the cross-sectional ovality of the laser-bent perforated tube is presented. The results indicate that the ovality increases with increasing LOP.

Increasing LOP results in more heat input and higher localized temperatures. This produces a larger temperature gradient between the outer and inner tube surfaces, leading to nonuniform thermal expansion across the wall thickness, which contributes to oval distortion of the cross-section. In addition, at higher power levels, the heat-affected region experiences uneven thermal stresses. The irradiated outer surface is subjected to tensile stresses, while the inner surface undergoes compressive stresses. This imbalance in circumferential stresses causes the tube's circular section to deform into an elliptical (oval) shape. In Fig. 9, the effect of LOP on the ovality percentage of holes located at the laser irradiating path of the laser-bent perforated tube is presented. As it is seen, the hole ovality percentage is increased with an increase in the LOP.

This is because increasing LOP raises the temperature difference between the irradiated and non-irradiated regions. This uneven heating causes non-uniform thermal expansion around the holes, deforming circular holes into an elliptical shape. At higher LOPs, localized melting or intense plastic deformation may occur near the hole edges. Material flow toward or away from the laser spot can further distort hole geometry, increasing hole ovality. In addition, the holes act as stress concentrators. With increasing LOP, the thermal stress developed unevenly, causing expansion or contraction in certain directions and resulting in elliptical distortion. Fig. 10 shows the effect of LOP on the TVR of the laser-bent perforated tube. As it is seen, the TVR increases with an increase in the LOP.

As LOP increases, the difference between thickening on the irradiated side and thinning on the opposite side increases. This occurs because higher power generates a stronger temperature difference through the tube wall, resulting in greater compressive strain on the laser side

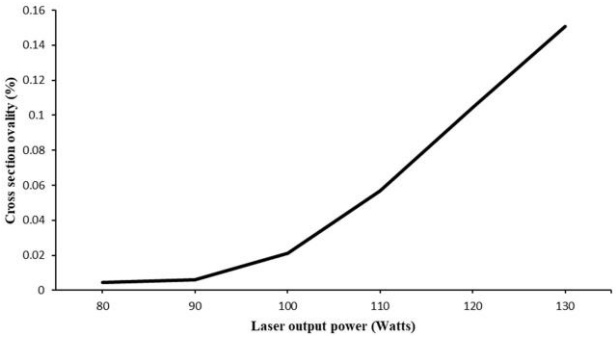

Fig. 8. The effect of LOP on the ovality percentage of cross-section of the laser-bent perforated tube.

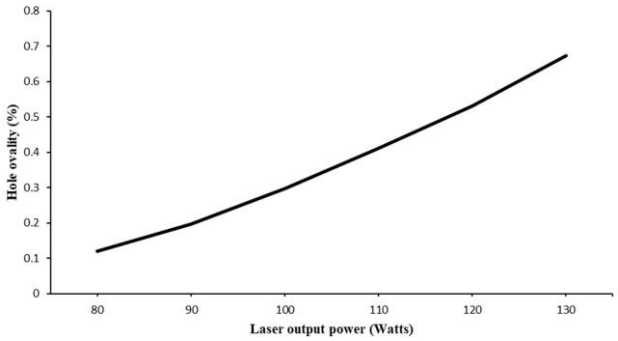

Fig. 9. Effect of LOP on the ovality percentage of holes located along the laser irradiating path of the laser-bent perforated tube.

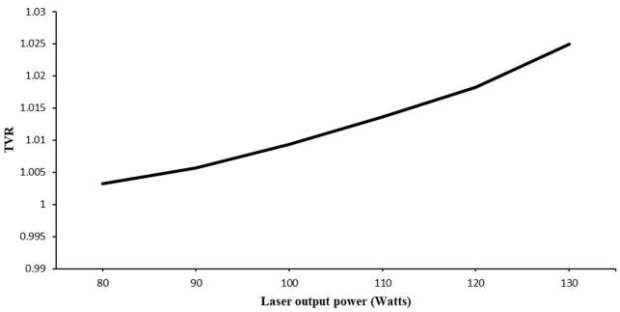

Fig. 10. Effect of LOP on the TVR of laser-bent perforated tube.

and higher tensile strain on the opposite side. Furthermore, the increased heat input softens a thicker layer of material, enabling more plastic flow from the cooler side toward the heated side.

3.2. The effect of LSS

In Fig. 11, the effect of LSS on the main displacement of the free edge of the laser-bent perforated tube is shown. As observed, the main displacement of the free edge decreases as the LSS increases.

In laser tube bending, increasing the LSS reduces the main displacement of the tube because the effective heat input delivered to the material is reduced. At higher scan speeds, the laser spends less time on each point, resulting in a lower absorbed energy density and a smaller temperature rise. Consequently, the thermal gradient and the size of the plastic deformation zone are reduced, while heat dissipates more rapidly through conduction. This reduction in heat input decreases the thermal expansion mismatch and the magnitude of compressive and tensile stresses across the tube wall, leading to a smaller overall bending angle.

In Fig. 12, the effect of LSS on the lateral displacement of the free edge of the laser-bent perforated tube is presented. As shown, the lateral displacement of the free edge decreases with increasing LSS.

The decrease in the lateral bending angle with increasing LSS is due to the reduction in thermal and mechanical asymmetry across the tube surface. At lower LSS values, the laser has a longer interaction time at each location, creating a highly non-uniform temperature distribution around the irradiated path. This uneven heating generates asymmetric thermal expansion, resulting in lateral deformation of the tube. When the LSS increases, the laser interaction time is reduced, heat has less time to accumulate, and the temperature field becomes more uniform. Consequently, the thermal stress imbalance between the two sides of the tube is reduced, leading to a smaller lateral bending angle.

In Fig. 13, the effect of LSS on the ovality percentage of cross-section of laser-bent perforated tube is shown. As observed, the ovality percentage decreases with increasing LSS.

The reduction of cross-sectional ovality at higher scan speeds is primarily due to the interplay between delivered thermal energy, local plastic flow, and mechanical constraints. As the scan speed increases, less heat is imparted to the bending zone, and the tube's outer layers experience a lower peak temperature, which restricts the metal's ability to flow plastically. Consequently, the material cannot expand outward as freely, limiting lateral deformation, and the cross-section remains closer to its original circular shape. Essentially, higher scan speeds reduce the time available for the metal

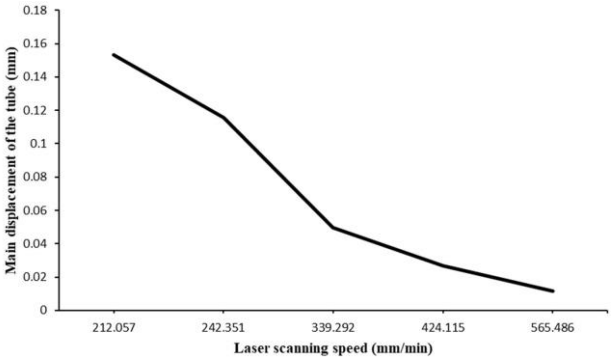

Fig. 11. The effect of LSS on the main displacement of free edge of laser-bent perforated tube.

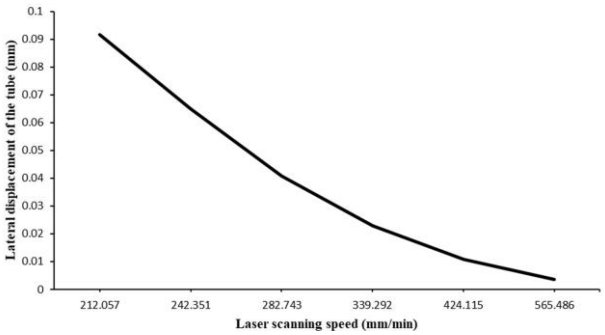

Fig. 12. The effect of LSS on the lateral displacement of free edge of laser-bent perforated tube.

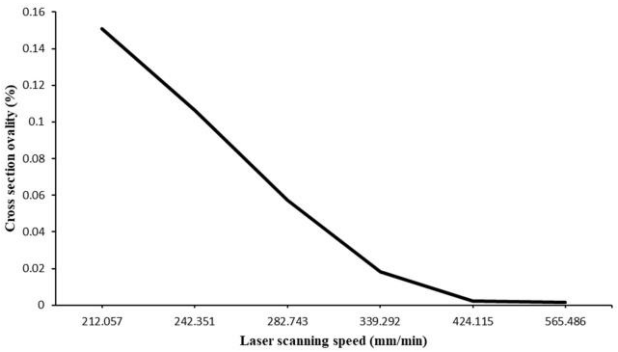

Fig. 13. The effect of LSS on the ovality percentage of cross-section of laser-bent perforated tube.

to undergo plastic deformation and ovalization, resulting in minimal cross-sectional distortion.

In Fig. 14, the effect of LSS on the ovality percentage of holes located at the laser irradiating path of the laser-bent perforated tube is presented. As observed, the hole ovality percentage decreases with increasing LSS.

The reduction in the ovality of holes located in the laser path with increasing scan speed is due to the decreased thermal energy delivered to the hole area and the reduced local plastic flow of the metal. At higher scan speeds, the laser spends less time on each point around the holes, and therefore the metal does not have enough opportunity to soften and flow laterally toward the hole edges. As a result, the holes retain a shape closer to their original circular form, and ovality is minimized.

In Fig. 15, the effect of LSS on the TVR of the laser-bent perforated tube is presented. As observed, the TVR decreases with increasing LSS.

The reduction in thickness differences across various areas in the laser path at higher scan speeds is caused by the decreased local plastic flow and reduced temperature gradients on the tube surface. At higher scan speeds, the metal has less opportunity to flow and locally thin or thicken relative to other regions. This results in smaller thickness variations between different areas, thereby maintaining a more uniform tube thickness. In other words, higher scan speeds preserve the metal closer to its original shape, minimizing thickness differences.

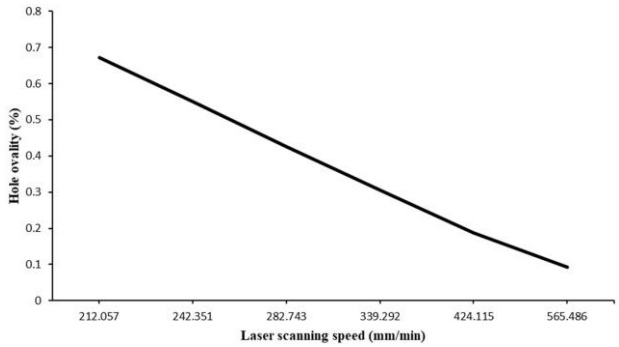

Fig. 14. Effect of LSS on the ovality percentage of holes located at the laser irradiating path of the laser-bent perforated tube.

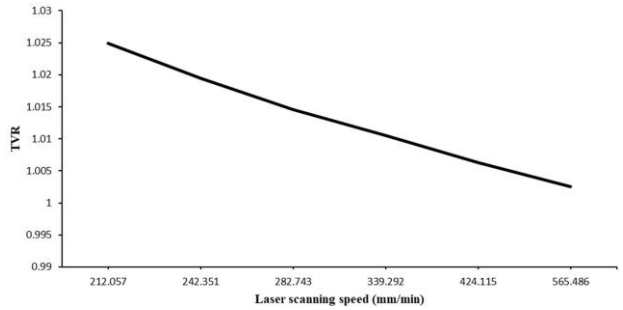

Fig. 15. Effect of LSS on the TVR of laser-bent perforated tube.

4. Conclusions

This investigation demonstrates that laser output power (LOP) and laser scan speed (LSS) are critical, opposing factors in the laser bending of perforated tubes. Increasing LOP raises heat input, which successfully increases the main bending displacement by creating a larger plastic deformation zone. However, higher power simultaneously increases undesirable lateral displacement, cross-sectional ovality, hole ovality, and thickness variation due to intensified and asymmetric thermal stresses. Conversely, increasing LSS reduces heat input per unit length, which decreases all measured distortions—main displacement, lateral displacement, both types of ovality, and thickness variation—by limiting thermal gradients and plastic flow. Therefore, the forming outcome represents a direct trade-off: greater bending angle is achieved only at the cost of increased geometric distortion, while higher scan speeds improve shape preservation at the expense of bending efficiency. This establishes that process parameters must be carefully balanced to achieve a target bend while minimizing collateral damage to the geometry of the tube and its perforations.

Finally, it should be noted that the conclusions are valid specifically for the geometry and laser irradiating pattern considered in the present study.

Authors' contributions

M. Safari: Conceptualization, Validation, Formal analysis, Visualization, Writing-original draft, Writing—review and editing, Supervision

D. Daneshpour: Methodology, Investigation, Data curation

Conflict of interest

The authors also acknowledge no conflict of interest.

Funding

The author hereby announces that no part of this study was funded by any institutions and/or organizations.

5. References

[1] Safari, M., Alves de Sousa, R., & Joudaki, J. (2023). Comprehensive assessment of laser tube bending process by response surface methodology. *Steel Research International*, *94*(2), 2200230. https://doi.org/10.1002/srin.202200230

[2] Imhan, K. I., Baharudin, B. T. H. T., Zakaria, A., Ismail, M. I. S. B., Alsabti, N. M. H., & Ahmad, A. K. (2018). Improve the material absorption of light and enhance the laser tube bending process utilizing laser softening heat treatment. *Optics & Laser Technology*, *99*, 15–18. https://doi.org/10.1016/j.optlastec.2017.09.038

[3] Hao, N. (2010, June). On the process parameter of laser tube bending. In *2010 International Conference on Mechanic Automation and Control Engineering* (pp. 5880–5883). IEEE. https://doi.org/10.1109/MACE.2010.5536120

[4] Imhan, K. I., Baharudin, B. T. H. T., Zakaria, A., Alsabti, N. M. H., & Ahmad, A. K. (2017). An analytical and experimental investigation of average laser power and angular scanning speed effects on laser tube bending process. In *MATEC Web of Conferences* (Vol. 95, p. 05008). EDP Sciences. https://doi.org/10.1051/matecconf/20179505008

[5] Imhan, K. I., Baharudin, B. T. H. T., Zakaria, A., Ismail, M. I. S. B., Alsabti, N. M. H., & Ahmad, A. K. (2017). Investigation of material specifications changes during laser tube bending and its influence on the modification and optimization of analytical modeling. *Optics & Laser Technology*, *95*, 151–156. https://doi.org/10.1016/j.optlastec.2017.04.001

[6] Guan, Y. J., Zhang, H. M., Sun, S., & Zhao, G. Q. (2011). Numerical study on influences of process parameters on laser tube bending. *Advanced Materials Research, 148*, 590–594. https://doi.org/10.4028/www.scientific.net/AMR.148-149.590

[7] Imhan, K. I., Baharudin, B. T. H. T., Zakaria, A., Ismail, M. I. S. B., Alsabti, N. M. H., & Ahmad, A. K. (2018). Features of laser tube bending processing based on laser forming: A review. *Journal of Lasers, Optics & Photonics, 5*(1), 1000174. https://doi.org/10.4172/2469-410X.1000174

[8] Hao, N. H., & Gai, Y. L. (2012). On the three-dimensional laser bending of metal tubes. *Applied Mechanics and Materials, 197*, 297–301. https://doi.org/10.4028/www.scientific.net/AMM.197.297

[9] Li, W., & Yao, Y. L. (2001). Laser bending of tubes: Mechanism, analysis, and prediction. *Journal of Manufacturing Science and Engineering, 123*(4), 674–681. https://doi.org/10.1115/1.1410120

[10] Khandandel, S. E., Seyedkashi, S. M. H., & Hoseinpour Gollo, M. (2020). Effect of cooling on bending angle and microstructure in laser tube bending with circumferential scanning. *Iranian Journal of Materials Forming, 7*(1), 14–23. https://doi.org/10.22099/ijmf.2019.34652.1137

[11] Li, F., Liu, S., Shi, A., Chu, Q., Shi, Q., & Li, Y. (2019). Research on laser thread form bending of stainless steel tube. *International Journal of Precision Engineering and Manufacturing, 20*, 893–903. https://doi.org/10.1007/s12541-019-00109-5

[12] Guan, Y., Yuan, G., Sun, S., & Zhao, G. (2013). Process simulation and optimization of laser tube bending. *The International Journal of Advanced Manufacturing Technology, 65*, 333–342. https://doi.org/10.1007/s00170-012-4181-8

[13] Zhang, P., & Liu, H. (2010, August). Thermal deformation behaviors of laser rectangular tube bending. In *2010 International Conference on Computer, Mechatronics, Control and Electronic Engineering* (Vol. 6, pp. 398–401). IEEE. https://doi.org/10.1109/CMCE.2010.5610615

[14] Safari, M. (2021). A study on main and lateral bending angles in laser tube bending process. *Journal of Stress Analysis. 5*(2), 33–40. https://doi.org/10.22084/jrstan.2021.23127.1163